Electronic Supplementary Material (ESI) for Journal of Materials Chemistry C.

Extended ligand conjugation and dinuclearity as a route to efficient platinum-based near-infrared (NIR) triplet emitters and solution-processed NIR-OLEDs

Marsel Z. Shafikov,* Piotr Pander, * Andrey Zaytsev, Ruth Daniels, Ross Martinscroft, Fernando B. Dias, J. A. Gareth Williams,* and Valery N. Kozhevnikov*

Supporting Information

Contents

1. Synthesis

Compound numbering is as shown in Scheme 1 of the main text

Synthesis of 3

A mixture containing 4,6-dichloropyrimidine (**1**) (184 mg, 1.24 mmol), 5′-hexyl-2,2′-bithiophene-5-boronic acid pinacol ester (**2**) (1.07 g, 2.84 mmol), $Pd(PPh_3)_4$ (86 mg, 74.4 µmol) and Cs_2CO_3 (2.42 g, 7.44 mmol) in 1,4-dioxane (40 mL) was deoxygenated with Ar for 10 min. The reaction mixture was heated to reflux for 16 h under argon atmosphere. Toluene (80 mL) was added and the resulting slurry was washed with water (3 × 20 mL). The organic layer was dried over $MgSO_4$; and the volatiles were removed under reduced pressure. The residue was dissolved in a minimum amount of ethyl acetate and precipitated by adding petroleum ether. The solid was collected by filtration to 4,6-bis[5-(5-hexylthiophen-2-yl)thiophen-2-yl]pyrimidine (**3**) (492 mg, 69%) as a yellow solid.

^{1}H NMR (400 MHz, $CDCl_3$): δ 9.00 (s, 1H, Ar-H), 7.71-7.70 (m, 3H, Ar-H), 7.16 (d, 2H, *J* = 4.1 Hz, Ar-H), 7.13 (d, 2H, *J* = 3.7 Hz, Ar-H), 6.73 (d, 2H, *J* = 3.7 Hz, Ar-H), 2.81 (t, 4H, *J* = 7.8 Hz, 2 × C*H*$_2$), 1.69 (p, 4H, *J* = 7.3 Hz, 2 × C*H*$_2$), 1.43-1.30 (m, 12H, 6 × C*H*$_2$), 0.90 (t, 6H, *J* = 6.9 Hz, 2 × C*H*$_3$). ^{13}C NMR (101 MHz, CD_2Cl_2): δ 159.0 (CH), 158.6 (quat.), 147.3 (quat.), 142.6 (quat.), 139.8 (quat.), 134.1 (quat.), 128.2 (CH), 125.3 (CH), 124.7 (CH), 124.0 (CH), 107.9 (CH), ~50.3 (CH_2, obscured by $CHDCl_2$), 31.6 (CH_2), 30.2 (CH_2), 28.8 (CH_2), 22.6 (CH_2), 13.9 (CH_3).

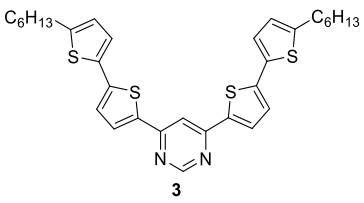

3

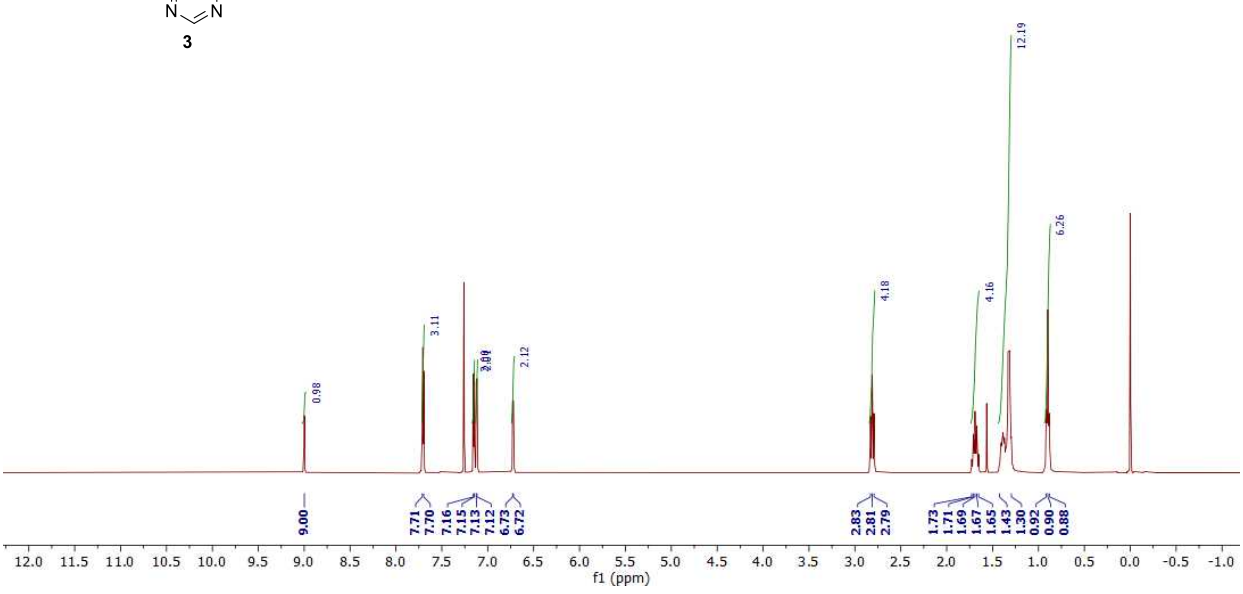

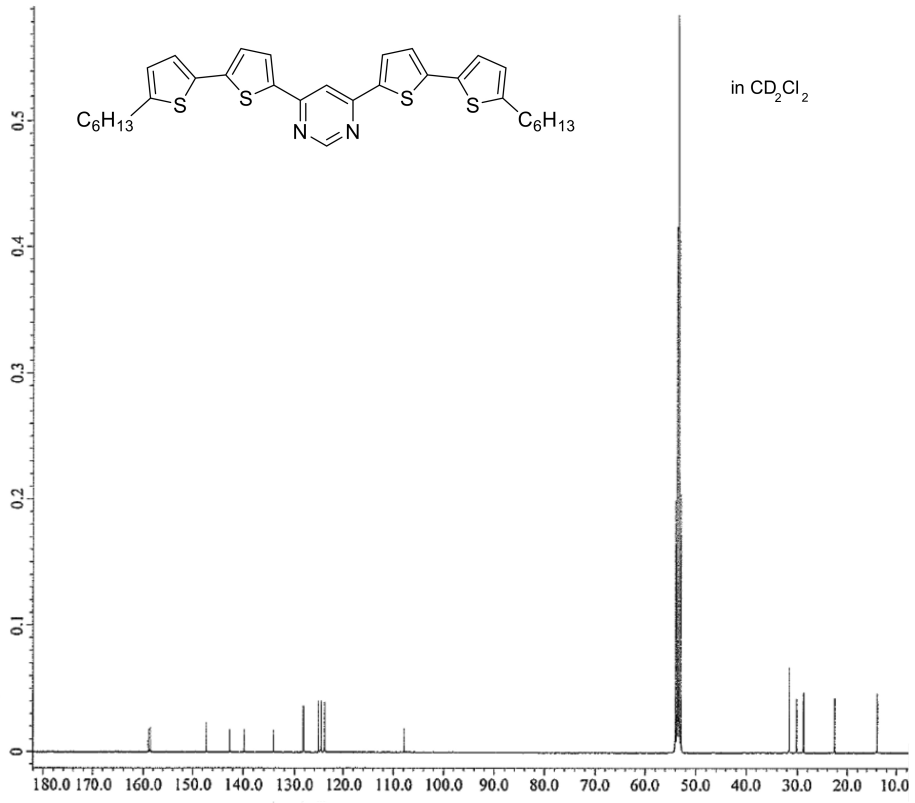

C-13 chemical shift / ppm

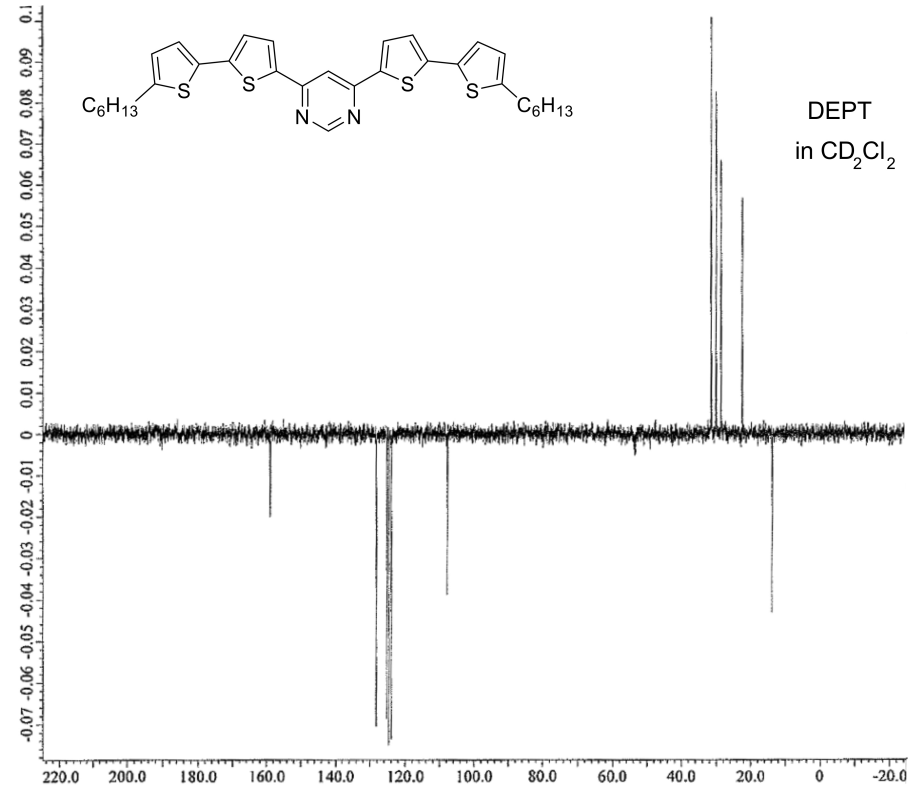

C-13 chemical shift / ppm

Synthesis of 4

To a solution of 4,6-bis[5-(5-hexylthiophen-2-yl)thiophen-2-yl]pyrimidine (**3**) (155 mg, 0.269 mmol) in acetic acid (40 mL), potassium tetrachloroplatinate (246 mg, 0.592 mmol) was added. The reaction mixture was heated to reflux under argon for 3 d. The reaction mixture was cooled to room temperature. The precipitated dichloro-bridged dimer was filtered and washed with methanol (5 mL), water (5 mL) and methanol (5 mL).

To the dichloro-bridged dimer (0.238 g, 0.233 mmol), DMSO (3 mL) was added. The reaction mixture was stirred at 130 °C for approximately 1.5 h and allowed to cool to room temperature. Water (30 mL) was added and the mixture was filtered. The solid collected was washed with water and purified by column chromatography (silica gel, DCM → DCM:MeOH). This product was further purified by column chromatography (silica gel, DCM → DCM:EtOAc 4:1 → DCM:MeOH 20:1) to give intermediate **4** (122 mg, 38% over two steps) as a dark-purple solid.

^{1}H NMR (400 MHz, $CDCl_3$): δ 10.39 (s, 1H, Ar-H), 7.56 (s, 2H, Ar-H), 7.03 (d, 2H, *J* = 3.7 Hz, Ar-H), 6.66 (s, 1H, Ar-H), 6.60 (d, 2H, *J* = 3.7 Hz, Ar-H), 3.66 (s. 12H, 2 × OS(C*H*$_3$)$_2$), 2.71 (t, 4H, *J* = 7.5 Hz, 2 × C*H*$_2$), 1.66 (app. p, 4H, 2 × C*H*$_2$), 1.41-1.29 (m, 12H, 6 × C*H*$_2$), 0.90 (t, 6H, *J* = 6.8 Hz, 2 × C*H*$_3$).

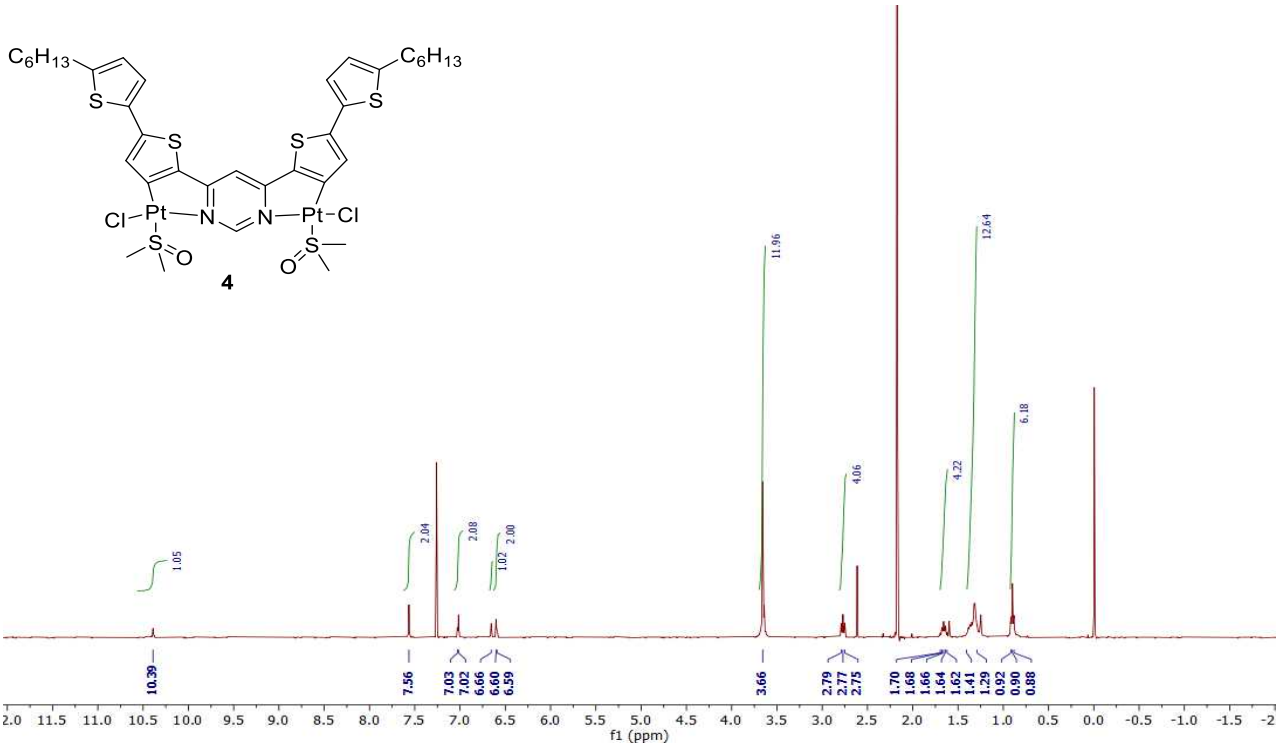

Synthesis of 5

A reaction mixture containing the DMSO complex **4** (217 mg, 0.1023 mol), Na_2CO_3 (217 mg, 2.05 mmol), 2,2,6,6-tetramethyl-3,5-heptadione (113 mg, 0.6138 mmol) and 2-ethoxyethanol (10 mL) was stirred at 130 °C for 16h under argon atmosphere. The reaction mixture was then cooled to room temperature and water (90 mL) was added. The resulting suspension was extracted with DCM (3 × 30 mL). Combined organic layers were dried over $MgSO_4$, and volatiles were removed under reduced pressure. The residue was purified by column chromatography (silica gel, DCM) to give the desired complex **5** (51 mg, 14%) as a dark-violet solid.

^{1}H NMR (400 MHz, $CDCl_3$): δ 9.06 (s, 1H, Ar-H), 7.20 (s, 2H), 7.16 (d, 2H, *J* = 3.6 Hz, Ar-H), 6.85 (s, 1H, Ar-H), 6.75 (d, 2H, *J* = 3.6 Hz, Ar-H), 5.86 (s, 2H, 2 × =C*H*), 2.83 (t, 4H, *J* = 7.6 Hz, 2 × CH_2), 1.70 (app. p, 4H, 2 × CH_2), 1.41-1.32 (m, 12H, 6 × CH_2), 1.28 (s, 18H, 2 × C(CH_3)$_3$), 1.27 (s, 18H, 2 × C(CH_3)$_3$), 0.90 (t, 6H, *J* = 6.9 Hz, 2 × CH_3).

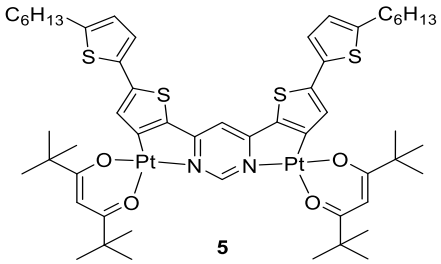

5

Elemental analysis of complex **5** was carried out on an ELEMENTAR vario MICRO CUBE instrument, and mass-spectrometry on a JEOL AccuTOF GCX instrument by field desorption (FD-MS), in both cases at the central analytical services of the University of Regensburg.

Elemental analysis of 5: Calculated for $C_{54}H_{72}N_2O_4Pt_2S_4$, %: C, 48.71; H, 5.45; N, 2.10. Found: C, 48.84; H, 5.41; N, 1.94.

FD-MS analysis of 5 ($C_{54}H_{72}N_2O_4Pt_2S_4$): Calculated For [$MH^+$]: 1331.3730. Found: 1331.3719.

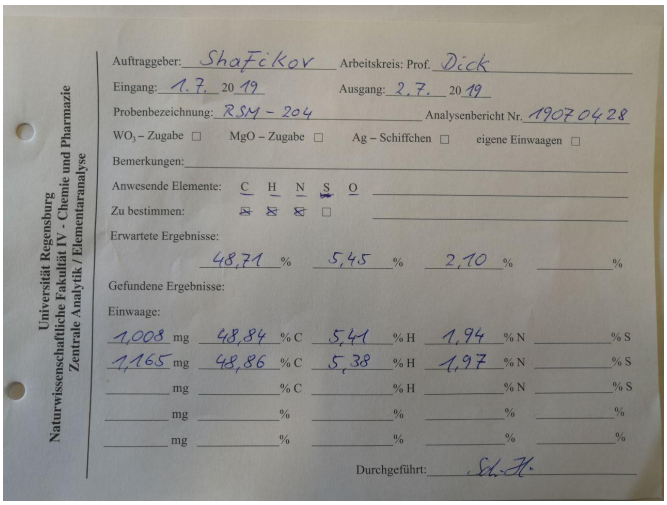

Universität Regensburg
Naturwissenschaftliche Fakultät IV - Chemie und Pharmazie
Zentrale Analytik / Elementaranalyse

Auftraggeber: ShaFikov Arbeitskreis: Prof. Dick
Eingang: 1.7. 2019 Ausgang: 2.7. 2019
Probenbezeichnung: RSM - 204 Analysenbericht Nr. 19070428
WO_3 – Zugabe ☐ MgO – Zugabe ☐ Ag – Schiffchen ☐ eigene Einwaagen ☐
Bemerkungen:
Anwesende Elemente: C H N S O
Zu bestimmen: ~~C~~ ~~H~~ ~~N~~ ☐
Erwartete Ergebnisse:
48,71 % 5,45 % 2,10 % %
Gefundene Ergebnisse:
Einwaage:

1,008 mg	48,84 % C	5,41 % H	1,94 % N	% S
1,165 mg	48,86 % C	5,38 % H	1,97 % N	% S
mg	% C	% H	% N	% S
mg	%	%	%	%
mg	%	%	%	%

Durchgeführt: Sch.

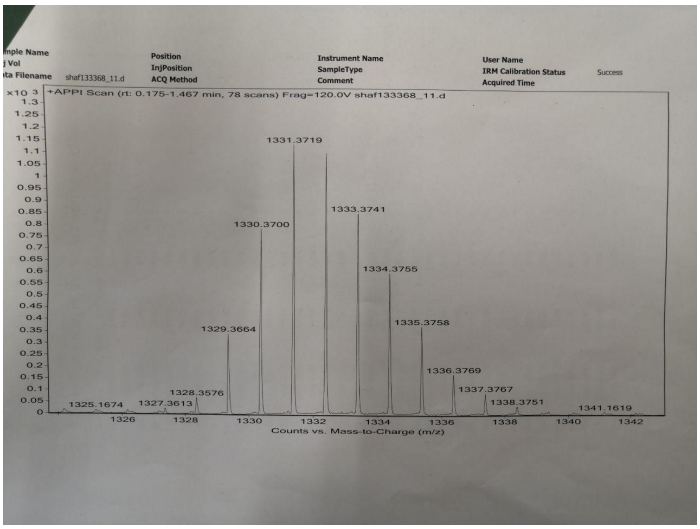

2. X-Ray Crystallography

Single, clear, orange, prism-shaped crystals of **5** were obtained by slow convectional diffusion of methanol into solution of **5** in dichloromethane. A suitable crystal ($0.32 \times 0.06 \times 0.03$) mm^3 was selected and mounted with inert oil onto a MITIGEN holder on a SuperNova diffractometer equipped with an Atlas CCD detector. The temperature of the crystal was maintained at 123.00(10) K during data collection. The structure was solved with the ShelXT 2018/3 (Sheldrick, 2015) structure solution program,[1] using the Intrinsic Phasing solution method and Olex2[2] as the graphical interface. The model was refined with version 2018/3 of ShelXL[1] using least squares minimization.

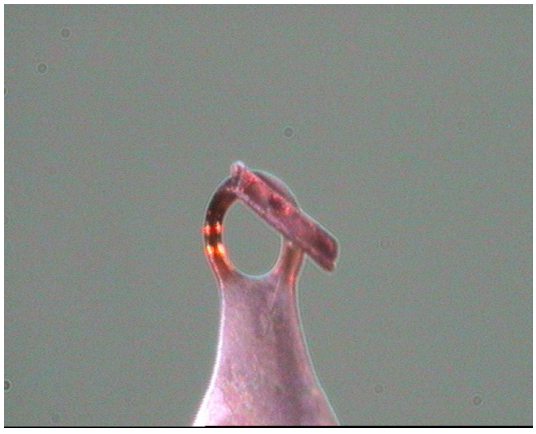

Table S1. Crystallographic data for **complex 5**.
CCDC deposition number: 1954414

Formula	$C_{54}H_{72}N_2O_4Pt_2S_4$
$D_{calc.}$/ g cm^{-3}	1.674
μ/mm^{-1}	11.595
Formula Weight	1331.55
Colour	dark red
Shape	needle
Size/mm^3	0.32×0.06×0.03
T/K	123.00(10)
Crystal System	monoclinic
Space Group	$I2/a$
a/Å	13.0080(2)
b/Å	29.9327(3)
c/Å	13.6224(2)
α/°	90
β/°	95.1120(10)
γ/°	90
V/Å^3	5282.98(12)
Z	4
Z'	0.5
Wavelength/Å	1.54184
Radiation type	CuK_α
Θ_{min}/°	3.577
Θ_{max}/°	76.403
Measured Refl.	35097
Independent Refl.	5518
Reflections with I > 2(I)	5309
R_{int}	0.0498
Parameters	410
Restraints	0
Largest Peak	1.531
Deepest Hole	-0.862
GooF	1.076
wR_2 (all data)	0.0548
wR_2	0.0542
R_1 (all data)	0.0216
R_1	0.0207

3. Optical spectroscopy

The UV-Vis absorption spectrum of complex **5** in toluene was measured with a Varian Cary 300 double beam spectrometer. The photoluminescence (PL) spectra and emission decay times of **5** in toluene solution and in doped polystyrene film were measured with a Horiba Jobin Yvon Fluorolog-3 steady-state fluorescence spectrometer, modified to allow for time-dependent measurements, for which the excitation source was a PicoBright PB-375 pulsed diode laser (λ_{exc} = 378 nm, pulse width 100 ps). The PL signal was detected with a cooled photomultiplier attached to a FAST ComTec multichannel scalar PCI card with a time resolution of 250 ps. The PL quantum yields were determined with a Hamamatsu C9920-02 system equipped with a Spectralon® integrating sphere.

4. Computations

All calculations were carried out with the Gaussian 09 package[3] utilizing the DFT approach with the M06 functional[4] and the def2-SVP basis set[5] including ECPs for the Pt atoms. The C-PCM solvation model[6] was applied with solvent parameters of toluene. Geometry optimizations were conducted with "tight" criteria.

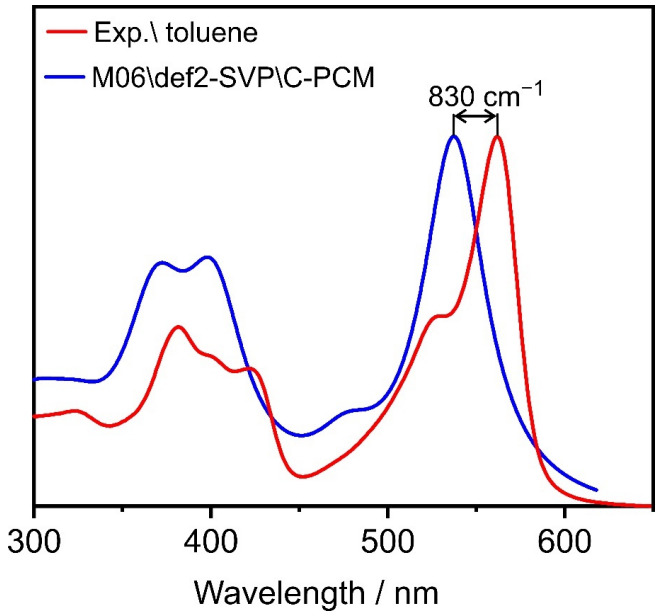

Figure S1. TD-DFT calculated absorption spectrum (blue) of the model complex **5'** in the optimized ground state geometry and the experimental spectrum of **5** in toluene (red).

Table S2. The coordination center bond lengths and angles of **5** derived from XRD measurement and of model complex **5'** at the DFT-optimized S_0 ground state and T_1 excited state geometries. The atom numbering corresponds to that given in Figure 2 of the main text.

Parameter	**5** XRD (esd)*	**5'** Ground state (S_0)	**5'** Emitting state (T_1)
Bonds (Å)			
Pt-C1	1.965(3)	1.9714	1.9716
Pt-N	2.0386(19)	2.0457	2.0366
Pt-O1	1.9916(17)	2.0300	2.0324
Pt-O2	2.0843(16)	2.1250	2.1271
N-C3	1.391(3)	1.3853	1.3957
Angles (degree^o)			
C1-Pt-N	81.67(9)	80.692	80.902
O1-Pt-O1	92.37(7)	91.121	90.933
C1-Pt-O1	89.21(9)	93.855	93.872
C1-Pt-O2	177.76(9)	175.023	175.195
N-Pt-O1	170.87(8)	174.545	174.773
N-Pt-O2	96.74(7)	94.332	94.294
Torsion angles (degree^o)			
C2-C1-Pt-O1	177.07(17)	179.678	180.000
C3-N-Pt-O2	174.29(15)	179.632	179.999
C1-C2-C3-N	3.0(2)	0.187	0.000
C6-C7-C8-S2	11.9(3)	0.027	0.001

*esd – estimated standard deviation is given in the parentheses.

Table S3. DFT calculated frontier orbital energies and atomic contributions of the model complex **5'** in the optimized T_1 state geometry resulting from Mulliken population analysis.

Orbitals	**Energy /eV**	**Contribution (Mulliken)**				
		Pt1	**Pt2**	**bis-dthpym**	**acac1**	**acac2**
LUMO+4	-0.7938	2	2	91	1	4
LUMO+3	-0.9996	1	1	2	63	33
LUMO+2	-1.1205	1	1	14	28	56
LUMO+1	-1.9591	1	1	98	0	0
LUMO	-2.7116	3	3	92	1	1
HOMO	-5.4920	6	4	87	2	1
HOMO-1	-5.8571	9	8	80	1	2
HOMO-2	-6.3517	27	0	32	41	0
HOMO-3	-6.4106	0	27	29	0	44
HOMO-4	-6.6490	88	2	6	4	0
HOMO-5	-6.6766	32	5	47	14	1
HOMO-6	-6.7237	2	88	6	0	4
HOMO-7	-6.7834	8	39	32	5	16

acac1 – acetylacetonate coordinated to Pt1 acac2 – acetylacetonate coordinated to Pt2

Table S4. TD-DFT calculated lowest triplet and singlet states of the model complex **5'** in the optimized T_1 state geometry.

State, Energy / eV	*f* (oscillator strength)	Transition (coefficient)*	Character**
triplets			
T_1 1.293	(triplet)	HOMO→LUMO (0.62) HOMO−1→LUMO (0.22) HOMO→LUMO+1 (-0.19) HOMO−1→LUMO+1 (-0.12)	$LC^{bis\text{-}dthpym}$ /$M^{Pt1/Pt2}L^{bis\text{-}dthpym}CT$
T_2 1.759	(triplet)	HOMO−1→LUMO (0.47) HOMO−1→LUMO+1 (0.25) HOMO→LUMO (-0.23) HOMO→LUMO+1 (-0.36)	$LC^{bis\text{-}dthpym}$/$M^{Pt1/Pt2}L^{bis\text{-}dthpym}CT$
T_3 2.404	(triplet)	HOMO→LUMO+1 (0.45) HOMO−1→LUMO (0.38) HOMO−3→LUMO (-0.19) HOMO−5→LUMO (0.17) HOMO−7→LUMO (0.15) HOMO−1→LUMO+3 (0.13) HOMO→LUMO+3 (0.10)	$LC^{bis\text{-}dthpym}$ /$M^{Pt1/Pt2}L^{bis\text{-}dthpym}CT$
singlets			
S_1 2.106	1.3118	HOMO→LUMO (0.70)	$LC^{bis\text{-}dthpym}$/$M^{Pt1/Pt2}L^{bis\text{-}dthpym}CT$
S_2 2.454	0.1545	HOMO−1→LUMO (0.68) HOMO−5→LUMO (0.13)	$LC^{bis\text{-}dthpym}$/$M^{Pt1/Pt2}L^{bis\text{-}dthpym}CT$/ $M^{Pt1}L^{bis\text{-}dthpym}CT$
S_3 2.906	0.0921	HOMO→LUMO+1 (0.68) HOMO−3→LUMO (-0.12)	$LC^{bis\text{-}dthpym}$/$M^{Pt1/Pt2}L^{bis\text{-}dthpym}$ CT/ $M^{Pt2}L^{bis\text{-}dthpym}CT$
S_4 2.980	0.2582	HOMO−3→LUMO (0.63) HOMO−1→LUMO+1 (-0.23) HOMO−5→LUMO (-0.13) HOMO→LUMO+1 (0.11)	$M^{Pt2}L^{bis\text{-}dthpym}CT/L^{acac2}L^{bis\text{-}dthpym}CT$/ $LC^{bis\text{-}dthpym}$
S_5 3.004	0.2575	HOMO−2→LUMO (0.65) HOMO→LUMO+2 (0.24) HOMO−1→LUMO+1 (-0.19) HOMO−2→LUMO+1 (0.11) HOMO−3→LUMO (0.10)	$M^{Pt1}L^{bis\text{-}dthpym}CT/L^{acac1}L^{bis\text{-}dthpym}CT$/ $LC^{bis\text{-}dthpym}$
S_6 3.011	0.0062	HOMO−6→LUMO (0.60) HOMO−4→LUMO (-0.35)	$M^{Pt2}L^{bis\text{-}dthpym}CT$/ $M^{Pt1}L^{bis\text{-}dthpym}CT$
S_7 3.046	0.0012	HOMO−4→LUMO (0.58) HOMO−6→LUMO (0.35) HOMO−4→LUMO+1 (0.16)	$M^{Pt1}L^{bis\text{-}dthpym}CT$/ $M^{Pt2}L^{bis\text{-}dthpym}CT$
S_8 3.111	0.0504	HOMO−1→LUMO+1 (0.51) HOMO−7→LUMO (-0.30) HOMO−3→LUMO (0.20) HOMO−5→LUMO (0.19) HOMO−2→LUMO (0.17)	$LC^{bis\text{-}dthpym}$/$M^{Pt1/Pt2}L^{bis\text{-}dthpym}CT$

S_9 3.234	0.2770	HOMO−7→LUMO (0.60) HOMO−1→LUMO+1 (0.26) HOMO−3→LUMO (0.16)	$M^{Pt2/Pt1}L^{bis\text{-}dthpym}CT/LC^{bis\text{-}dthpym}$
S_{10} 3.297	0.2719	HOMO−5→LUMO (0.62) HOMO−1→LUMO+1 (-0.23) HOMO−2→LUMO (-0.11) HOMO−1→LUMO (-0.11) HOMO→LUMO+1 (0.10)	$M^{Pt1/Pt2}L^{bis\text{-}dthpym}$ $CT/LC^{bis\text{-}dthpym}$
S_{11} 3.657	0.0000	HOMO−11→LUMO (0.61) HOMO−9→LUMO (-0.31)	$M^{Pt2/Pt1}L^{bis\text{-}dthpym}CT$
S_{12} 3.676	0.1142	HOMO−2→LUMO+1 (0.62) HOMO→LUMO+2 (0.25) HOMO−2→LUMO (-0.10)	$M^{Pt1}L^{bis\text{-}dthpym}CT/L^{acac1}L^{bis\text{-}dthpym}CT/$ $LC^{bis\text{-}dthpym}$
S_{13} 3.707	0.0000	HOMO−9→LUMO (0.60) HOMO−11→LUMO (-0.31) HOMO−9→LUMO+1 (-0.16)	$M^{Pt1/Pt2}L^{bis\text{-}dthpym}CT$

*Square of the given coefficient multiplied by two gives percentage contribution of the corresponding transition to formation of the excited state.

**LC – Ligand Centered; MLCT – Metal to Ligand Charge Transfer; LLCT – Ligand to Ligand Charge Transfer.

Table S5. DFT optimized ground state (S_0) and T_1 state geometries of the model complex **5'** in cartesian (*xyz*) coordinates of the atoms of atomic number indicated in the first column

S_0				T_1			
8	-4.898983000	-2.063935000	0.025127000	8	4.878505000	-2.069550000	-0.000020000
6	-5.208507000	-3.301002000	0.047548000	6	5.185339000	-3.307177000	-0.000033000
6	-4.329148000	-4.392605000	0.057390000	6	4.303024000	-4.396761000	-0.000052000
6	-2.920138000	-4.354089000	0.039475000	6	2.893950000	-4.353373000	-0.000059000
8	-2.205672000	-3.309490000	0.018781000	8	2.183036000	-3.306512000	-0.000047000
78	-3.002668000	-1.339649000	0.005423000	78	2.983250000	-1.335716000	-0.000025000
78	3.002701000	-1.339474000	-0.012775000	78	-3.009430000	-1.343764000	0.000007000
8	2.206499000	-3.309554000	-0.027905000	8	-2.190209000	-3.304931000	0.000037000
6	2.921452000	-4.354061000	-0.033483000	6	-2.893261000	-4.357374000	0.000075000
6	4.330522000	-4.392302000	-0.027246000	6	-4.301649000	-4.412964000	0.000099000
6	5.209431000	-3.300283000	-0.016274000	6	-5.195178000	-3.331982000	0.000084000
8	4.899308000	-2.063204000	-0.010041000	8	-4.902631000	-2.091526000	0.000047000
6	6.686192000	-3.552707000	-0.011082000	6	-6.668432000	-3.605770000	0.000112000
6	2.165422000	-5.648384000	-0.050147000	6	-2.120896000	-5.642171000	0.000096000
6	-1.199755000	0.953504000	-0.013586000	6	1.190518000	0.964923000	-0.000031000
7	-1.169706000	-0.431454000	-0.010008000	7	1.158891000	-0.430386000	-0.000028000
6	-0.000059000	-1.054142000	-0.010927000	6	-0.015448000	-1.055376000	-0.000024000
7	1.169570000	-0.431411000	-0.013064000	7	-1.182556000	-0.440651000	-0.000025000
6	1.199484000	0.953569000	-0.012997000	6	-1.214252000	0.959528000	-0.000034000
6	-0.000157000	1.660926000	-0.015231000	6	-0.004817000	1.669075000	-0.000037000
6	2.525017000	1.460062000	-0.008697000	6	-2.521013000	1.471053000	-0.000033000
6	-2.525355000	1.459855000	-0.013097000	6	2.517098000	1.467454000	-0.000023000
16	-3.059657000	3.119174000	-0.019563000	16	3.061635000	3.123255000	-0.000012000
6	-3.580736000	0.545082000	-0.005254000	6	3.569377000	0.546771000	-0.000013000
6	3.580461000	0.545356000	-0.004609000	6	-3.624174000	0.522849000	-0.000016000
6	4.828197000	1.206240000	0.003017000	6	-4.833976000	1.169865000	-0.000013000
6	4.723668000	2.588634000	0.004941000	6	-4.746931000	2.592473000	-0.000026000
16	3.059176000	3.119435000	-0.002860000	16	-3.029179000	3.127385000	-0.000045000
6	-4.828532000	1.205899000	-0.004426000	6	4.820464000	1.199863000	0.000003000

6	-4.724117000	2.588287000	-0.011675000	6	4.726273000	2.583236000	0.000004000
6	5.786671000	3.563865000	0.013268000	6	-5.758928000	3.547296000	-0.000024000
6	-5.787197000	3.563468000	-0.013540000	6	5.792952000	3.552324000	0.000021000
6	-2.164285000	-5.648605000	0.034011000	6	2.132776000	-5.645021000	-0.000082000
6	-6.685129000	-3.553807000	0.063729000	6	6.661406000	-3.564484000	-0.000027000
16	7.457619000	3.053092000	0.035442000	16	-7.461406000	3.085564000	-0.000004000
6	8.027160000	4.693531000	0.036172000	6	-7.970391000	4.755995000	-0.000013000
6	6.973444000	5.574059000	0.020140000	6	-6.880363000	5.609386000	-0.000030000
6	5.707215000	4.940311000	0.007222000	6	-5.643469000	4.954798000	-0.000037000
6	-5.707731000	4.939911000	-0.020295000	6	5.720858000	4.929888000	0.000001000
6	-6.974041000	5.573622000	-0.020181000	6	6.990410000	5.557015000	0.000032000
6	-8.027838000	4.693070000	-0.013337000	6	8.040132000	4.671631000	0.000077000
16	-7.458267000	3.052651000	-0.006917000	16	7.462253000	3.033452000	0.000081000
6	-9.484655000	4.992232000	-0.011172000	6	9.498406000	4.963387000	0.000118000
6	9.483874000	4.992722000	0.053057000	6	-9.412724000	5.102698000	-0.000001000
1	-4.789512000	-5.383578000	0.077009000	1	4.760564000	-5.389256000	-0.000063000
1	4.791411000	-5.383198000	-0.032355000	1	-4.749804000	-5.409709000	0.000133000
1	7.141112000	-3.066022000	-0.888419000	1	-7.125813000	-3.131977000	0.883228000
1	6.938669000	-4.620766000	-0.017630000	1	-6.905840000	-4.677312000	0.000156000
1	7.132546000	-3.079047000	0.877728000	1	-7.125835000	-3.132045000	-0.883028000
1	1.491603000	-5.685298000	0.820468000	1	-1.462662000	-5.667665000	-0.882978000
1	2.818157000	-6.530875000	-0.041466000	1	-2.762155000	-6.533080000	0.000118000
1	1.524821000	-5.680158000	-0.945937000	1	-1.462652000	-5.667631000	0.883163000
1	-0.000116000	-2.151569000	-0.009416000	1	-0.010609000	-2.152934000	-0.000018000
1	-0.000177000	2.754182000	-0.016252000	1	-0.003980000	2.762912000	-0.000041000
1	5.790813000	0.686008000	0.006912000	1	-5.800238000	0.655388000	-0.000001000
1	-5.791121000	0.685635000	0.001455000	1	5.779724000	0.673268000	0.000012000
1	-1.595822000	-5.728014000	-0.906767000	1	1.474937000	-5.676645000	0.883080000
1	-1.424547000	-5.641834000	0.849674000	1	1.474918000	-5.676601000	-0.883232000
1	-6.937125000	-4.621800000	0.084421000	1	6.910626000	-4.633363000	-0.000047000
1	-7.142900000	-3.089424000	-0.824175000	1	7.113605000	-3.085696000	0.883070000
1	-7.129040000	-3.058209000	0.941710000	1	7.113619000	-3.085658000	-0.883096000
1	7.116622000	6.657631000	0.017816000	1	-6.998045000	6.696116000	-0.000038000
1	4.755584000	5.478926000	-0.006537000	1	-4.675753000	5.463264000	-0.000051000
1	-4.756031000	5.478558000	-0.025183000	1	4.771834000	5.473235000	-0.000036000
1	-7.117220000	6.657186000	-0.025006000	1	7.138974000	6.639926000	0.000022000
1	10.001700000	4.572834000	-0.825164000	1	-9.932162000	4.698761000	0.885754000
1	9.979423000	4.580836000	0.947788000	1	-9.932181000	4.698743000	-0.885736000
1	9.642421000	6.081164000	0.050171000	1	-9.539453000	6.195156000	-0.000010000
1	-2.813090000	-6.528351000	0.134394000	1	2.781971000	-6.530198000	-0.000110000
1	-9.643183000	6.080669000	-0.016166000	1	9.662509000	6.051052000	0.000113000
1	-9.989182000	4.580728000	0.878692000	1	10.003341000	4.544981000	-0.886384000
1	-9.993605000	4.571952000	-0.894393000	1	10.003286000	4.544998000	0.886660000

5. Electrochemistry

Cyclic voltammetry was conducted in three-electrode, one-compartment cell in nitrogen atmosphere. All measurements performed in 0.1 M Bu_4NBF_4 (99%, Sigma Aldrich, dried) in dichloromethane (ExtraDry AcroSeal®, Acros Organics). Electrodes: working (Pt disc with 1 mm diameter), counter (Pt wire), reference (Ag/AgCl calibrated against ferrocene). All cyclic voltammetry measurements performed at room temperature with scan rate of 50 mV s^{-1}. Ionization potential (IP) and electron affinity (EA) were determined from respective *onset* potentials using a well-known relation:[7,8] IP = E_{onset}^{ox} + 5.1; EA = E_{onset}^{red} + 5.1. Here E_{onset}^{ox} denotes the onset oxidation potential, and E_{onset}^{red} the onset reduction potential.

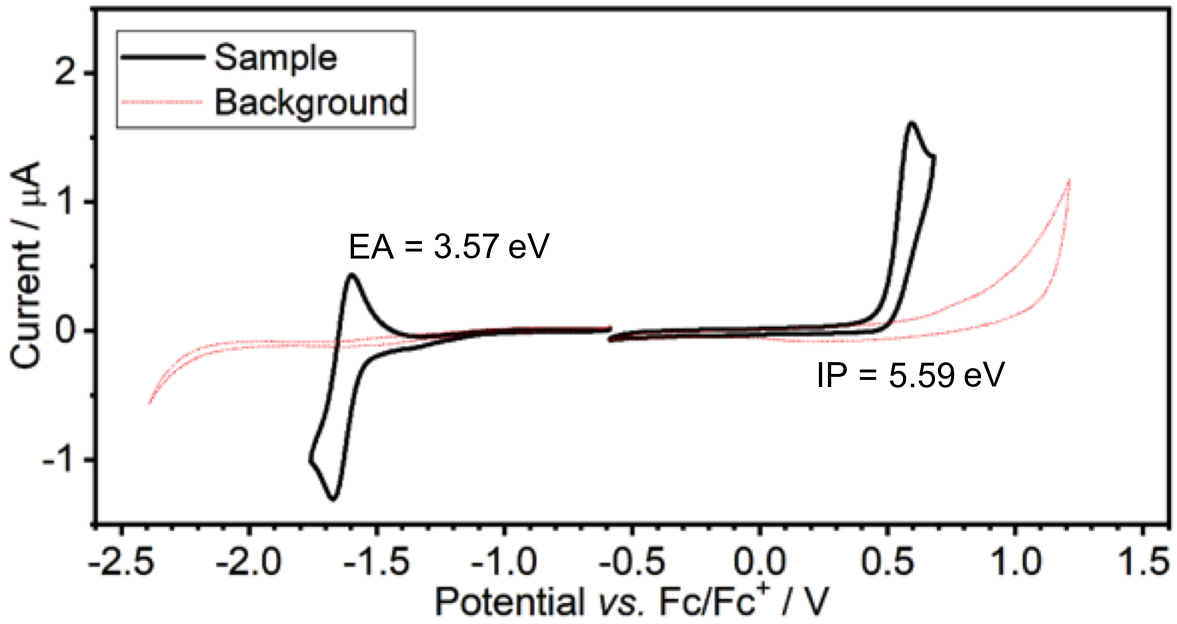

Figure S2. Electrochemical oxidation and reduction signals recorded with cyclic voltammetry in 0.1 M Bu_4NBF_4 / CH_2Cl_2 supporting electrolyte solution. Note: all potentials are referenced against half wave potential of the ferrocene/ferrocenium redox couple.

The electrochemical redox behavior of the **5** is no different from the typical picture of Pt(II) complexes: with reversible reduction and irreversible oxidation.[9,10] The oxidation onset potential E_{onset}^{ox} = 0.49 V while for reduction E_{onset}^{red} = -1.51 V and $E_{1/2}^{red}$ = -1.63 V relatively to the Fc/Fc^+ half wave potential. E_{onset}^{ox} and E_{onset}^{red} correspond to Ionization potential, IP = 5.59 eV, and electron affinity, EA = 3.57 eV, respectively. Electrochemical reduction and oxidation processes can be ascribed, in majority, to the ligand due to its strong contribution to the molecular frontier orbitals as has been discussed in the optical spectroscopy section and shown by DFT calculations (Figure 6). The electrochemical energy gap E_g^{el} = 2.06 eV is very similar to the optical gap in CH_2Cl_2, E_g^{el} = 2.09 eV derived from the mostly π-π* absorption band λ_{max} = 563 nm (the onset at λ_{onset} = 602 nm) and correlates well with the TD-DFT calculated S_1 state energy of 2.1 eV (Table S4).

6. Photophysics in films

Absorption spectra of solutions were recorded with UV-3600 double beam spectrophotometer (Shimadzu). Photoluminescence (PL) spectra of solutions were recorded using a QePro compact spectrometer (Ocean Optics). PL quantum yields (Φ_{PL}) in the solid state were determined with a method described earlier[11] using an integrating sphere (Labsphere) coupled with a QePro spectrometer (Ocean Optics) and a LED light source (Ocean Optics). PL spectra in the solid state were recorded using the same set of integrating sphere and detector. Time-resolved photoluminescence spectra and decay traces were recorded using nanosecond gated luminescence and lifetime measurements (from 400 ps to 1 s) using the third harmonic of a high-energy pulsed Nd:YAG laser (EKSPLA), λ_{ex} = 355 nm. Emission was focused onto a spectrograph and detected on a sensitive gated iCCD camera (Stanford Computer Optics) with sub-nanosecond resolution. Time resolved measurements were performed by exponentially increasing gate and integration times. Temperature-dependent experiments were conducted using a liquid nitrogen cryostat (Janis Research) with sample in flowing vapour, while measurements at room temperature were recorded in vacuum in the same cryostat. Power dependence data were fitted according to a linear relationship between intensity and power per pulse. Further details of the iCCD setup and measurements can be found elsewhere.[12]

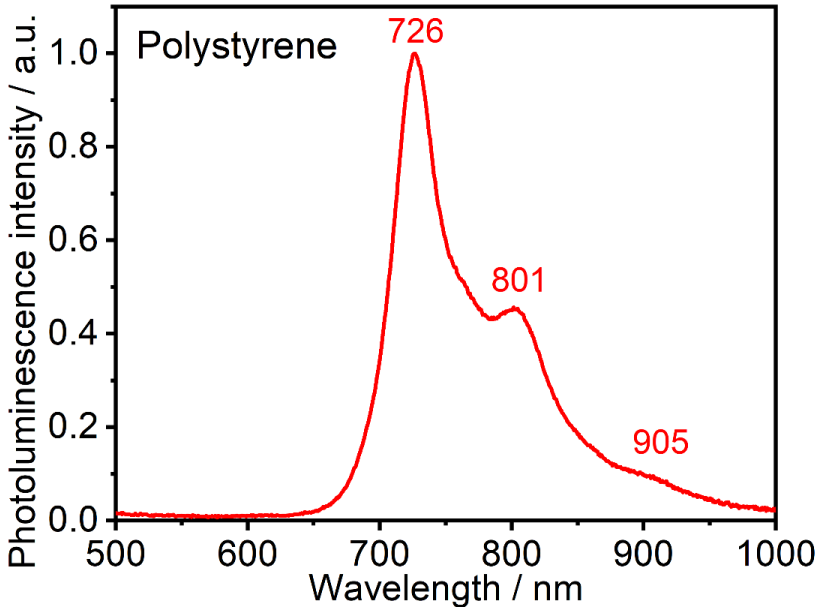

Figure S3. Normalised photoluminescence spectrum of **5** doped in polystyrene film. Numbers in red indicate position (in nanometres) of specific features of the spectrum, such as maximum or shoulder.

Photophysical behaviour in OLED hosts

The choice of host in a solution-processed device is based on several factors, some of them being good solubility and perfect film-forming properties. A blend of a hole transport material (TCTA, TPD) and an electron transport material (PO-T2T, PBD) has been chosen to satisfy the hole and electron confinement as well as the above-mentioned properties. The TPD:PBD host has provided good results when used in a multilayer device in combination with the related complex **Pt_2(bit-thpym)(acac)$_2$** (Figure 1 in the main text).[13] With **5,** however, TPD:PBD shows minor residual emission in the OLED (Figure S4, bottom). The sole occurrence of host's emission in electroluminescence indicates that the bulk of recombination occurs on the host rather than at the dopant. Increasing host-to-guest energy transfer should eliminate the problem. With this objective in mind, another host was explored, TCTA:PO-T2T. It shows an emission spectrum perfectly matching the strong, low-energy absorption band of **5** (Figure S4, top). Indeed, Device 1, using TCTA:PO-T2T as host shows a lower proportion of host emission in comparison to Device 2 with the TPD:PBD host.

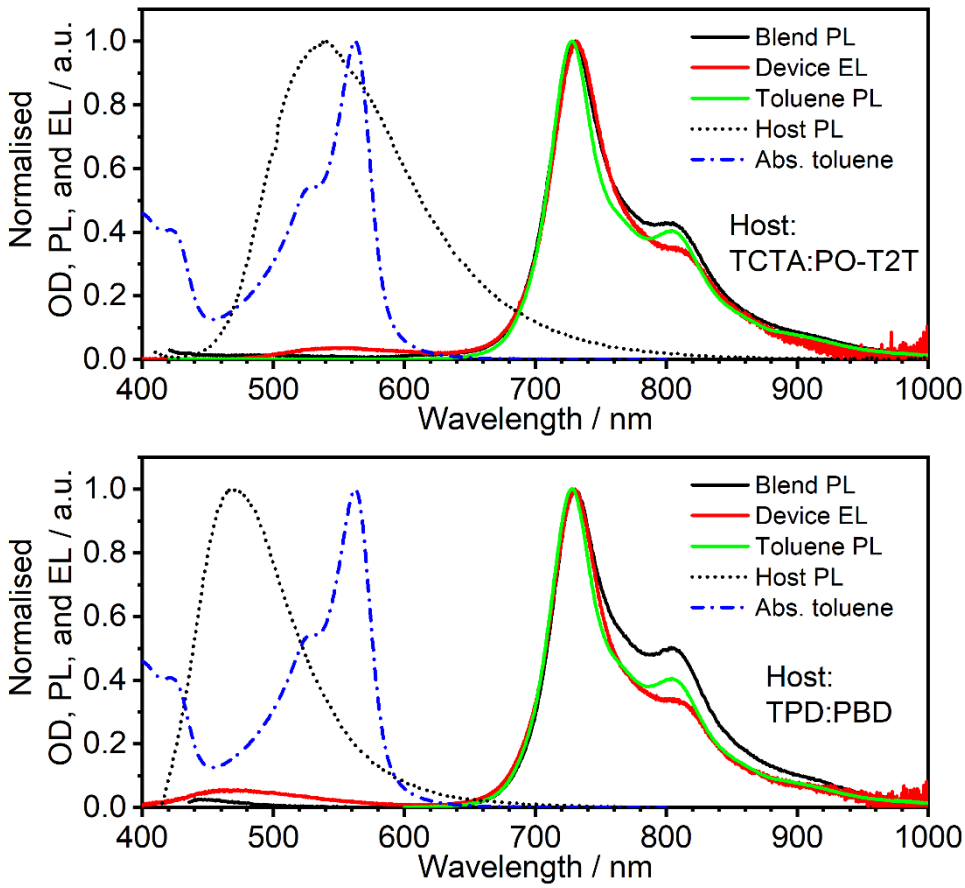

Figure S4. Photoluminescence (PL) spectra of **5** in OLED host (top: TCTA:PO-T2T, bottom: TPD:PBD) compared with the electroluminescence spectrum and the PL spectrum in toluene at 10^{-5} M. The absorption spectrum of **5** in toluene and the emission spectra of each of the blend hosts in film are also shown.

As shown in Figure S5, TCTA:PO-T2T shows two decay components of which one is related to prompt fluorescence (≈ 0-100 ns delay), while the other (≈ 1-100 µs) to delayed fluorescence. This delayed fluorescence component shows a linear power dependence (Figure S6), which conclusively indicates that thermally activated delayed fluorescence (TADF) is occurring. On the contrary, TPD:PBD at room temperature shows only a prompt fluorescence component (≈ 0-500 ns delay), with and additional phosphorescence component being observed at 80 K at longer delays (≈ 1-100 ms delay).

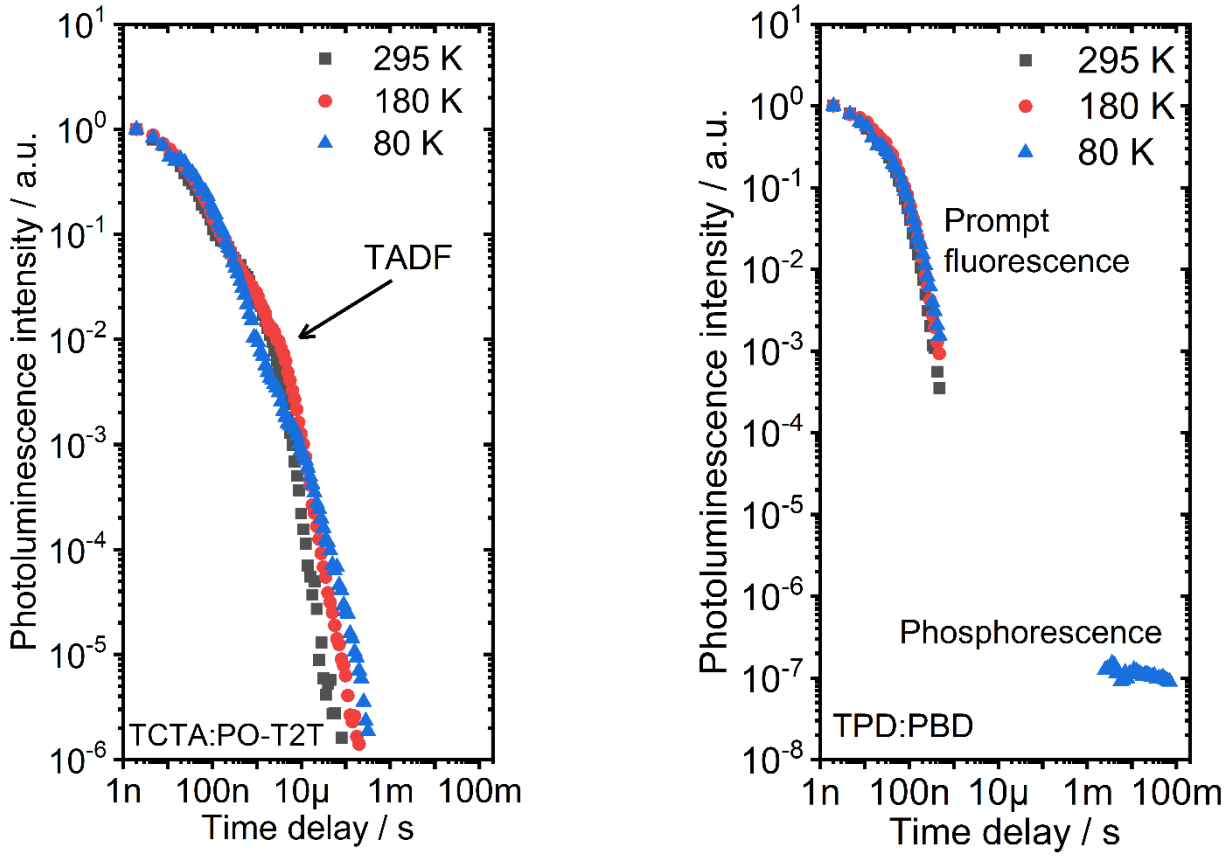

Figure S5. Photoluminescence decay of blend hosts at various temperatures: TCTA:PO-T2T (left), TPD:PBD (right). Note the second exponential component of the TCTA:PO-T2T decay indicated as thermally activated delayed fluorescence (TADF).

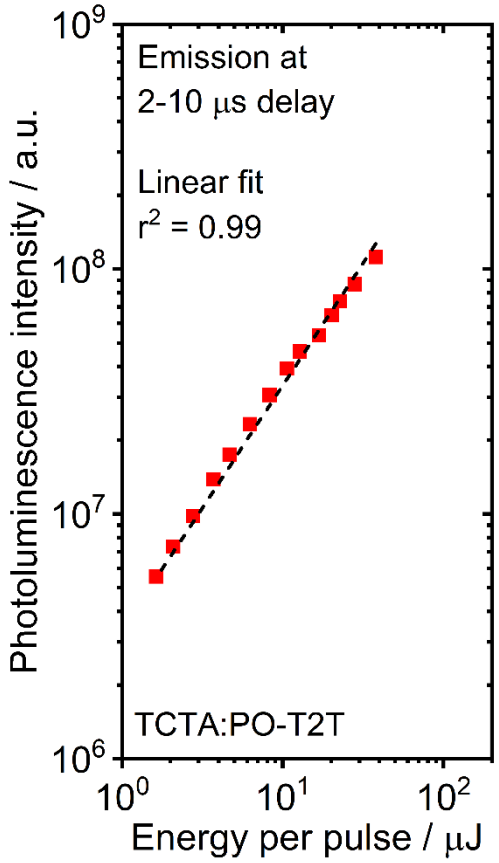

Figure S6. Relation between excitation pulse energy and delayed fluorescence intensity.

Typically, TADF compounds or exciplexes show phosphorescence emission at lower temperatures due to the thermally-activated nature of the $T_1 \rightarrow S_1$ reverse intersystem crossing. However, in TCTA:PO-T2T, no conclusive evidence for phosphorescence at 80 K is found and the long-lived emission at this temperature is attributed to TADF (Figure S7). This behaviour is indicative of a nearly negligible singlet–triplet gap, $\Delta E_{ST} \approx 0$. The behaviour of TPD:PBD is typical of a fluorescent exciplex, while the phosphorescence spectrum observed at 80 K matches that of TPD's triplet emission (Figure S8).[14] Finally, given the results presented above, the lowest triplet-state energy of the two hosts can be established to be approximately 2.7 eV in TCTA:PO-T2T exciplex (treating the S_1/T_1 states of the exciplex as nearly isoenergetic) and 2.43 eV in TPD:PBD (T_1 of TPD). Both values are above the T_1 energy of **5** of 1.78 eV.

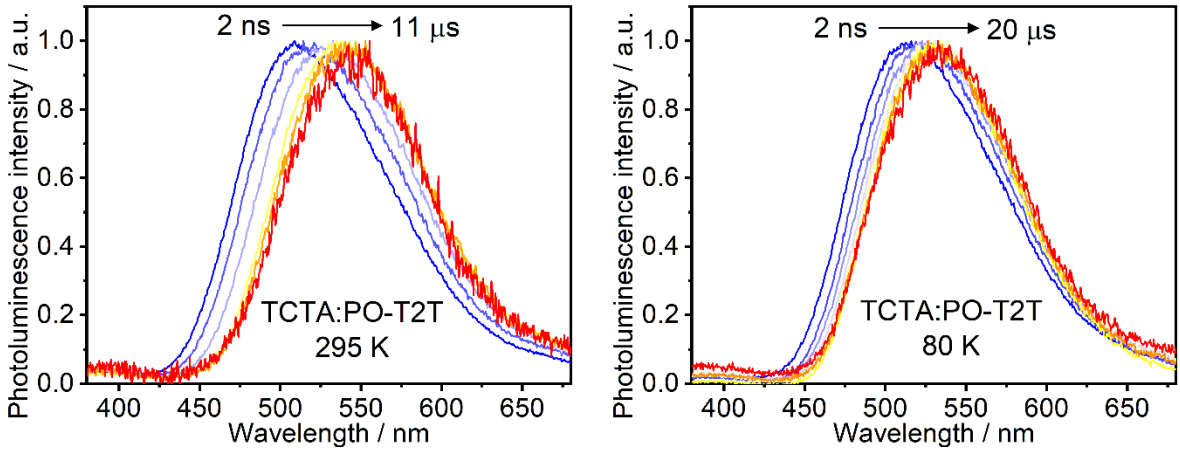

Figure S7. Selected time-resolved photoluminescence spectra of undoped TCTA:PO-T2T blend: 295 K (left) and 80 K (right). Spectra recorded over indicated time delay after excitation with exponential intervals.

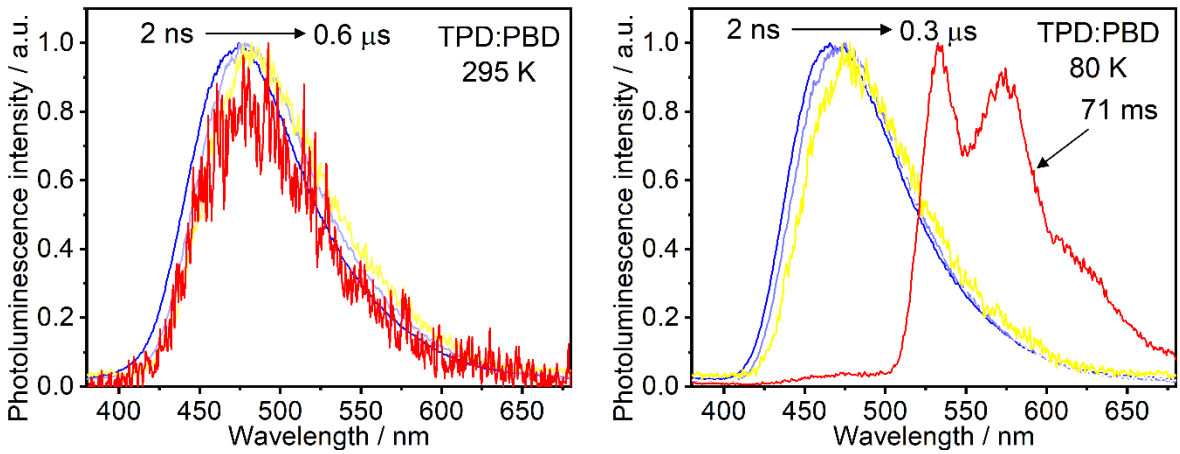

Figure S8. Selected time-resolved photoluminescence spectra of undoped TCTA:PO-T2T blend: 295 K (left) and 80 K (right). Spectra recorded over indicated time delay after excitation with exponential intervals.

The time-resolved study of **5**-host interaction (Figure S9) shows that the hosts' fluorescent decay is faster in a **5**-doped film than in undoped film, suggesting a significant role of Förster energy transfer. In a **5**:TCTA:PO-T2T blend, apart from prompt fluorescence of the host being quenched, nearly all delayed fluorescence is quenched as well. The PL decay of **5** in OLED host is biexponential and does not significantly change with temperature. The average PL lifetime at room temperature is identical for both OLED hosts: τ_{av} = 7.5 ± 0.9 μs in TCTA:PO-T2T and τ_{av} = 7.4 ± 0.5 μs in TPD:PBD. This value is smaller than that recorded in polystyrene by about 25% and stays in agreement with the lower Φ_{PL} recorded in these hosts. The lifetime recorded at

80 K is slightly larger than at room temperature: τ_{av} = 8.7 ± 1.5 μs in TCTA:PO-T2T and τ_{av} = 10.2 ± 2.4 μs in TPD:PBD.

The average photoluminescence lifetime (τ_{av}) is obtained using equation S1[15]:

$$\tau_{av} = \frac{A_1\tau_1^2 + A_2\tau_2^2}{A_1\tau_1 + A_2\tau_2} \quad \text{(S1)}$$

Where τ_1, τ_2 are decay constants and A_1, A_2 are pre-exponential amplitudes.

The long-lived component seen in the photoluminescence decay of **5** in TPD:PBD at 80 K is attributed to slow decay of traps (*i.e.* host T_1 state dissociated hole-electron pairs), in this case *via* energy transfer from metastable trap (higher energy) to the emitter (lower energy), and also known as non-geminate hole-electron pair recombination or long persistent luminescence.[14,16,17]

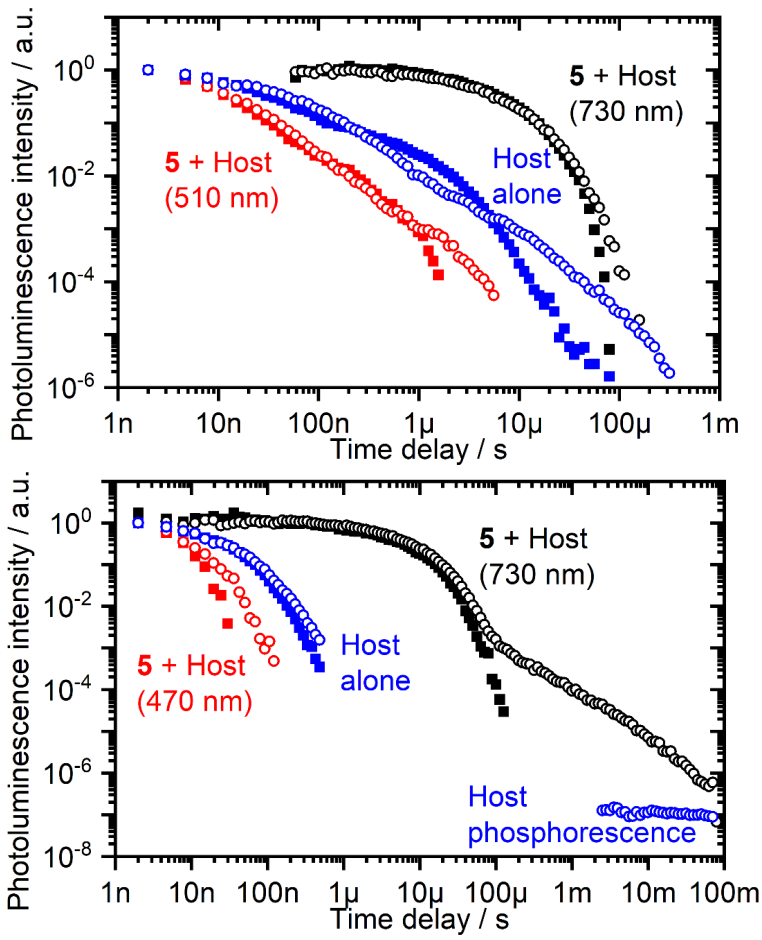

Figure S9. Photoluminescence decay of doped and undoped host in thin film, top: TCTA:PO-T2T, bottom: TPD:PBD. Full squares represent the decay at 295 K, while hollow circles represent decay at 80 K. Black – decay of **5** NIR emission (730 nm); red – decay of host's emission at the prompt fluorescence maximum; blue – decay of undoped host.

7. OLED devices

OLEDs were fabricated by spin-coating / evaporation hybrid method. The hole injection layer (Heraeus Clevios HIL 1.3N), electron blocking/hole transport layer (PVKH), and emitting layer (TPD:PBD or TCTA:PO-T2T + dopant) were spin-coated, whereas the electron transport layer (TPBi or PO-T2T) and cathode (LiF/Al) were evaporated. Devices of 4 x 2 mm pixel size were fabricated. The materials TPD = *N*,*N*'-bis(3-methylphenyl)-*N*,*N*'-diphenylbenzidine (sublimed, LUMTEC); TCTA = (tris(4-carbazoyl-9-ylphenyl)amine) (sublimed, LUMTEC); PO-T2T = 2,4,6-Tris[3-(diphenyl-phosphinyl)phenyl]-1,3,5-triazine (sublimed, LUMTEC); PVKH = poly(9-vinylcarbazole) (MW = 100000, Sigma Aldrich); PBD = 2-(biphenyl-4-yl)-5-(4-*tert*-butylphenyl)-1,3,4-oxadiazole (99%, Sigma Aldrich); TPBi - 2,2',2"-(1,3,5-benzinetriyl)-tris(1-phenyl-1-*H*-benzimidazole) (sublimed, LUMTEC); LiF (99.995%, Sigma Aldrich); and Aluminium wire (99.999%, Alfa Aesar) were purchased from the companies indicated in parentheses. OLED devices were fabricated using pre-cleaned indium-tin-oxide (ITO) coated glass substrates after ozone plasma treatment with a sheet resistance of 20 Ω cm^{-2} and ITO thickness of 100 nm. Heraeus Clevios HIL 1.3N was spun-coated and annealed onto a hotplate at 200 ºC for 3 min to give a 45 nm film. Electron blocking/hole transport layer (PVKH, 3 mg/mL), was spun from chloroform:chlorobenzene (95:5 v/v) mixture and annealed at 50 ºC for 5 min to give 10 nm film. The TPD:PBD layer was spun from a toluene solution of TPD:PBD (60:40 w/w) of total concentration of 10 mg/mL (TPD+PBD+emitter). The TCTA:PO-T2T layer was spun from TCTA:PO-T2T (70:30 w/w) solution in chloroform:chlorobenzene (95:5 v/v) mixture of total concentration of 20 mg/mL (TCTA+PO-T2T+emitter). The dopant was dissolved in the solution of hosts in order to obtain 5% weight contribution in the final layer. The solution was spun onto the PVKH layer and then annealed at 50 ºC for 5 min giving 30 ± 5 nm film (TPD:PBD) or directly onto HIL 1.3N (TCTA:PO-T2T) giving a 70 ± 5 nm film. All solutions were filtered using a PVDF syringe filter with 0.45 µm pore size. All other organic and inorganic layers were thermally evaporated using Kurt J. Lesker Spectros II deposition system at 10^{-6} mbar. All organic materials and aluminum were deposited at a rate of 1 Å s^{-1}. The LiF layer was deposited at 0.1-0.2 Å s^{-1}. Characterisation of OLED devices was conducted in a 10 inch integrating sphere (Labsphere) connected to a Source Measure Unit. Further experimental details can be found in previously published literature.[18]

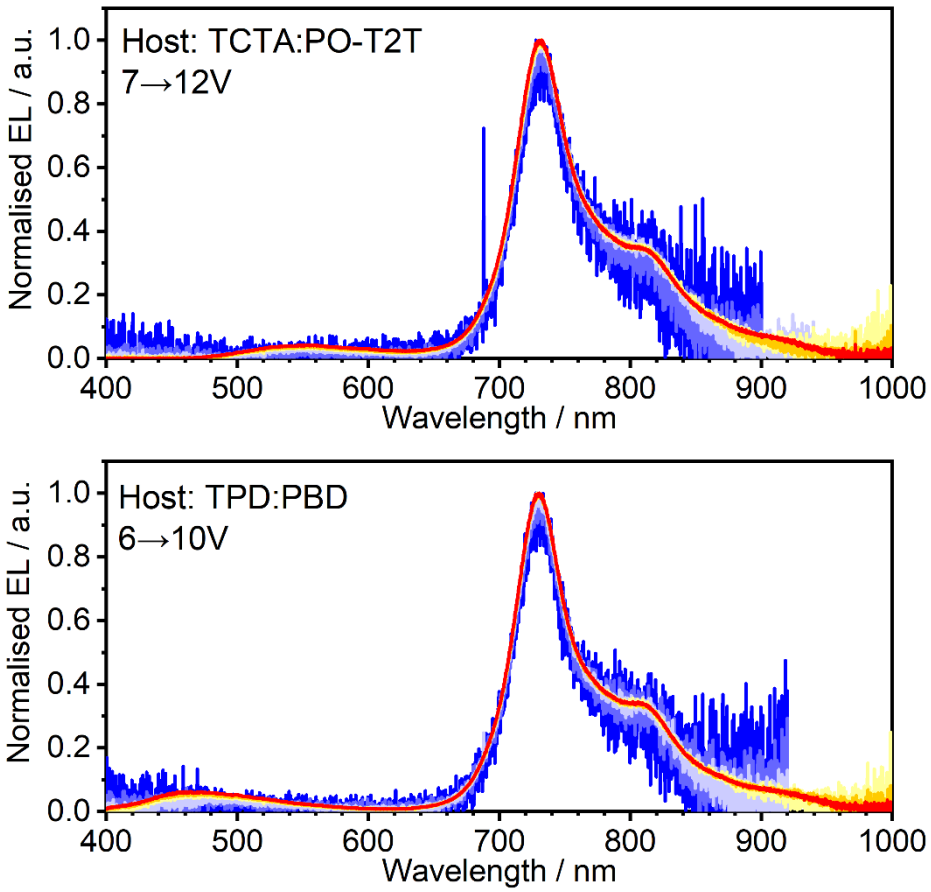

Figure S10. Normalised electroluminescence (EL) spectra of Devices 1 and 2 (top and bottom) at various voltage.

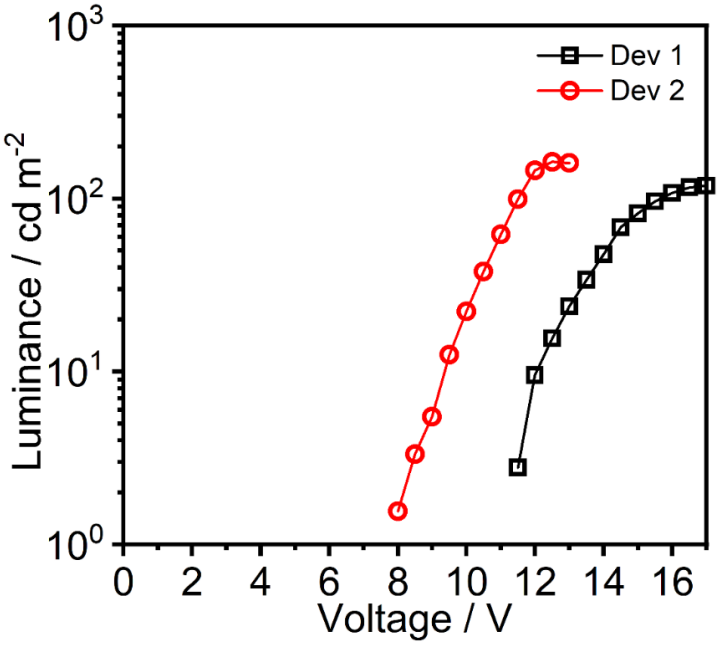

Figure S11. Luminance (≈ 390-700 nm) of devices 1 and 2 in function of applied voltage. Dominating NIR emission at >700 nm does not contribute to luminance.

8. References

(1) Sheldrick, G. SHELXT - Integrated space-group and crystal-structure determination. *Acta Cryst. A* **2015,** *71*, 3-8.

(2) Dolomanov, O. V.; Bourhis, L. J.; Gildea, R. J.; Howard, J. A. K.; Puschmann, H. OLEX2: a complete structure solution, refinement and analysis program. *J. Appl. Cryst.* **2009,** *42*, 339-341.

(3) Frisch, M. J.; Trucks, G. W.; Schlegel, H. B.; Scuseria, G. E.; Robb, M. A.; Cheeseman, J. R.; Scalmani, G.; Barone, V.; Mennucci, B.; Petersson, G. A.; Nakatsuji, H.; Caricato, M.; Li, X.; Hratchian, H. P.; Izmaylov, A. F.; Bloino, J.; Zheng, G.; Sonnenberg, J. L.; Hada, M.; Ehara, M.; Toyota, K.; Fukuda, R.; Hasegawa, J.; Ishida, M.; Nakajima, T.; Honda, Y.; Kitao, O.; Nakai, H.; Vreven, T.; Montgomery Jr., J. A.; Peralta, J. E.; Ogliaro, F.; Bearpark, M. J.; Heyd, J.; Brothers, E. N.; Kudin, K. N.; Staroverov, V. N.; Kobayashi, R.; Normand, J.; Raghavachari, K.; Rendell, A. P.; Burant, J. C.; Iyengar, S. S.; Tomasi, J.; Cossi, M.; Rega, N.; Millam, N. J.; Klene, M.; Knox, J. E.; Cross, J. B.; Bakken, V.; Adamo, C.; Jaramillo, J.; Gomperts, R.; Stratmann, R. E.; Yazyev, O.; Austin, A. J.; Cammi, R.; Pomelli, C.; Ochterski, J. W.; Martin, R. L.; Morokuma, K.; Zakrzewski, V. G.; Voth, G. A.; Salvador, P.; Dannenberg, J. J.; Dapprich, S.; Daniels, A. D.; Farkas, Ö.; Foresman, J. B.; Ortiz, J. V.; Cioslowski, J.; Fox, D. J. *Gaussian 09*. Gaussian, Inc.: Wallingford, CT, USA, 2009.

(4) Zhao, Y.; Truhlar, D. G. The M06 suite of density functionals for main group thermochemistry, thermochemical kinetics, noncovalent interactions, excited states, and transition elements: two new functionals and systematic testing of four M06-class functionals and 12 other functionals. *Theor. Chem. Acc.* **2008,** *120*, 215-241.

(5) Weigend, F.; Ahlrichs, R. Balanced basis sets of split valence, triple zeta valence and quadruple zeta valence quality for H to Rn: Design and assessment of accuracy. *Phys. Chem. Chem. Phys.* **2005,** *7*, 3297-3305.

(6) Cossi, M.; Rega, N.; Scalmani, G.; Barone, V. Energies, structures, and electronic properties of molecules in solution with the C-PCM solvation model. *J. Comput. Chem.* **2003,** *24*, 669-681.

(7) Cardona, C. M.; Li, W.; Kaifer, A. E.; Stockdale, D.; Bazan, G. C. Electrochemical Considerations for Determining Absolute Frontier Orbital Energy Levels of Conjugated Polymers for Solar Cell Applications. *Adv. Mater.* **2011,** *23*, 2367-2371.

(8) Pander, P.; Data, P.; Turczyn, R.; Lapkowski, M.; Swist, A.; Soloducho, J.; Monkman, A. P. Synthesis and characterization of chalcogenophene-based monomers with pyridine acceptor unit. *Electrochim. Acta* **2016,** *210*, 773-782.

(9) Brooks, J.; Babayan, Y.; Lamansky, S.; Djurovich, P. I.; Tsyba, I.; Bau, R.; Thompson, M. E. Synthesis and Characterization of Phosphorescent Cyclometalated Platinum Complexes. *Inorg. Chem.* **2002,** *41*, 3055-3066.

(10) Kvam, P.-I.; Puzyk, M. V.; Balashev, K. P.; Songstad, J. Spectroscopic and Electrochemical Properties of Some Mixed-Ligand Cyclometalated Platinum(II) Complexes Derived from 2-Phenylpyridine. *Acta Chem. Scand.* **1995,** *49*, 335-343.

(11) de Mello, J. C.; Wittmann, H. F.; Friend, R. H. An improved experimental determination of external photoluminescence quantum efficiency. *Adv. Mater.* **1997,** *9*, 230-232.

(12) Pander, P.; Data, P.; Dias, F. B. Time-resolved Photophysical Characterization of Triplet-harvesting Organic Compounds at an Oxygen-free Environment Using an iCCD Camera. *J. Vis. Exp* **2018**, e56614.

(13) Shafikov, M. Z.; Daniels, R.; Pander, P.; Dias, F. B.; Williams, J. A. G.; Kozhevnikov, V. N. Dinuclear Design of a Pt(II) Complex Affording Highly Efficient Red Emission: Photophysical Properties and Application in Solution-Processible OLEDs. *ACS Appl. Mater. Interfaces* **2019,** *11*, 8182-8193.

(14) Chapran, M.; Pander, P.; Vasylieva, M.; Wiosna-Salyga, G.; Ulanski, J.; Dias, F. B.; Data, P. Realizing 20% External Quantum Efficiency in Electroluminescence with Efficient Thermally Activated Delayed Fluorescence from an Exciplex. *ACS Appl. Mater. Interfaces* **2019,** *11*, 13460-13471.

(15) Lakowicz, J. R. *Principles of Fluorescence Spectroscopy*. Springer US: 2006.

(16) Kabe, R.; Adachi, C. Organic long persistent luminescence. *Nature* **2017,** *550*, 384-387.

(17) Pander, P.; Bulmer, R.; Martinscroft, R.; Thompson, S.; Lewis, F. W.; Penfold, T. J.; Dias, F. B.; Kozhevnikov, V. N. 1,2,4-Triazines in the Synthesis of Bipyridine Bisphenolate ONNO Ligands and Their Highly Luminescent Tetradentate Pt(II) Complexes for Solution-Processable OLEDs. *Inorg. Chem.* **2018,** *57*, 3825-3832.

(18) de Sa Pereira, D.; Monkman, A. P.; Data, P. Production and Characterization of Vacuum Deposited Organic Light Emitting Diodes. *J. Vis. Exp* **2018**, e56593.